

Second-Order Nonlinear Polarization in the Strong-Field Regime

Liang Li^{1,a}, Tengfei Huang^{1,a}, Pengfei Lan^{1,†}, Yinfu Zhang¹, Jiapeng

Li¹, Xiaosong Zhu¹, Lixin He¹, Wei Cao¹, and Peixiang Lu^{1,2,3‡}

¹*Wuhan National Laboratory for Optoelectronics and School of Physics,
Huazhong University of Science and Technology, Wuhan 430074, China*

²*Hubei Key Laboratory of Optical Information and Pattern Recognition,
Wuhan Institute of Technology, Wuhan 430205, China*

³*CAS Center for Excellence in Ultra-intense Laser Science, Shanghai 201800, China*

We theoretically and experimentally investigate the second-harmonic generation (SHG) in a strong laser field. Our prototype experiment with ZnO demonstrate distinct anisotropic distributions of SHG yield, which deviate from the normal perturbation nonlinear optics theory. The experimental results show that the second-order nonlinear susceptibility is no longer a constant and it changes in the strong-field regime. The new features of SHG are due to the so far overlooked polarization induced by strong-field tunneling. To reveal its effect, we propose a non-perturbation bond-charge model and a generalized second-order susceptibility (GSOS). Our work extends the normal second-order nonlinear responses from the perturbation to strong-field regime, and it suggests an all-optical approach to control the nonlinear optical properties of matter.

^a These authors contribute equally to this work

[†] Corresponding author: pengfeilan@hust.edu.cn

[‡] Corresponding author: lupeixiang@hust.edu.cn

Nonlinear polarization of materials induced by laser fields is the basis for manipulating the electronic and optical properties with light. Since the observation of second harmonic generation (SHG) in 1961 [1], interest in nonlinear optics has grown continuously, ranging from fundamental studies to applications such as laser frequency conversion and nonlinear microscopy, switching, etc. The nonlinear responses are generally described in terms of a power series in the electric field based on the perturbation theory [2–5] (we call it normal nonlinear optics for discriminating from the following discussion in the strong laser fields), e.g., the second-order polarization $\mathbf{P}^{(2)} = \chi^{(2)}\mathbf{E}\mathbf{E}$, where \mathbf{E} is the driving electric field, and $\chi^{(2)}$ is the second-order susceptibility.

With the development of laser techniques, the laser intensity can be stronger than the Coulomb field between the valence electron and nucleus (the laser intensity $\sim 10^{13}$ W/cm²). Subject to such a strong field, high-order harmonic generation can be observed in gases [6, 7], solids [8–13], and liquids [14]. High-order harmonic spectra generally exhibit nonperturbative behaviors and form a broad plateau structure, which has promoted the generation of attosecond pulses. In the past several decades, normal nonlinear optics and strong-field physics have greatly advanced the development of optics and created revolutionary changes in photonic technology [15]. Previously, these two fields almost develop parallelly. The former concentrates on the few-photon process, e.g., second-, third-harmonic generation, four-wave mixing, at moderate intensity, and the latter on the multi-photon process, e.g., high-order harmonic generation, multiphoton or tunneling ionization, at high intensity. However, the intersection between the normal nonlinear optics and strong field physics were essentially overlooked before.

In this Letter, we concentrate on the intersection of these two fields, i.e., second-order nonlinear polarization in an ultrashort strong laser pulse. The ultrashort laser pulses permit damage-free exposure of solids to strong laser intensity and provide a possible way to control the electric and optical properties of semiconductors [16–23]. We find that the orientation dependencies of SHG yield of ZnO crystal show different anisotropic distributions with increasing the laser intensity and wavelength. At lower intensity, the results can be well described by normal nonlinear optics theory. However, with increasing the laser intensity and wavelength, the SHG shows distinct anisotropic distributions that deviate from with the normal nonlinear optics theory. To explain these results, we propose a non-perturbation bond-charge model (NPBCM) and a generalized second-order susceptibility

(GSOS) in strong fields. It is shown that the electrons within nearby bonds can be coupled by the quantum tunneling, which induce an additional polarization. Moreover, the tunneling induced polarization increases exponentially with the laser intensity, and becomes dominant in the strong field regime.

The experiment is carried out with a near-infrared (800 nm or 2300 nm) linearly polarized laser pulse. We adopt a Ti:sapphire laser, which delivers a 35-fs, 800-nm pulse at a repetition rate of 1 kHz, with the maximum pulse energy of 7 mJ. The signal and idler infrared pulses are generated with an optical parametric amplifier (TOPAS-Prime-Plus, Coherent) pumped by the Ti:sapphire laser. The maximum pump energy is 5 mJ and the maximum output energy is about $600\mu\text{J}$ for the signal and $500\mu\text{J}$ for the idle pulses. The wavelength of the signal and idler pulses can be changed from 1200 nm to 2600 nm. The polarization direction and intensity of the laser pulses are controlled by the half-wave plate and wire-grid polarizer. The laser beam is normally focused on a $350\text{-}\mu\text{m}$ -thick, $(11\bar{2}0)$ ZnO crystal (see Fig. 1(a)), and the SHG is measured with the spectrometer by rotating the ZnO crystal. The spot size at the focal point is estimated to be $50\mu\text{m}$, and $125\mu\text{m}$ for the 2300-nm and 800-nm lasers, respectively, by using the knife-edge measurement. The polarization of the second harmonic is analyzed by using a wire-grid polarizer. The second harmonic of the 2300-nm pulse is spectrally resolved by a fiber grating spectrometer (NIRQuest 512 and USB4000, Ocean Optics), that of the 800-nm pulse is resolved by a spectrometer (SpectraPro HRS-300, Princeton Instruments) and a CCD camera (PI-MAX4, Princeton Instruments).

Figure 1(b)-1(d) shows the orientation dependence of SHG yield with the 2300-nm laser. Considering the symmetry of the system, only the results from 0° to 180° are shown. At lower intensity ($0.4\text{ TW}/\text{cm}^2$), the orientation dependence of the SHG from 0° to 180° shows a unimodal structure with a peak at 90° , i.e., “8” structure from 0° to 360° . This structure agrees well with the prediction of the normal perturbation theory. With increasing the laser intensity, the orientation dependence of the SHG is first changed to a unimodal structure with a flattop at $1.6\text{ TW}/\text{cm}^2$ (fat “8” structure), and then even to a double-peak structure (butterfly structure) at a higher intensity ($2.6\text{ TW}/\text{cm}^2$). We also plot the intensity dependence of SHG at four typical orientations 0° , 45° , 60° , and 90° in Fig. 1(e). Note that such an intensity scaling can be reproduced by varying the laser intensity from low value to high value and vice versa as long as the maximum intensity is lower than the damage threshold (see Sec. I in the supplementary information). One can see that, when the laser intensity

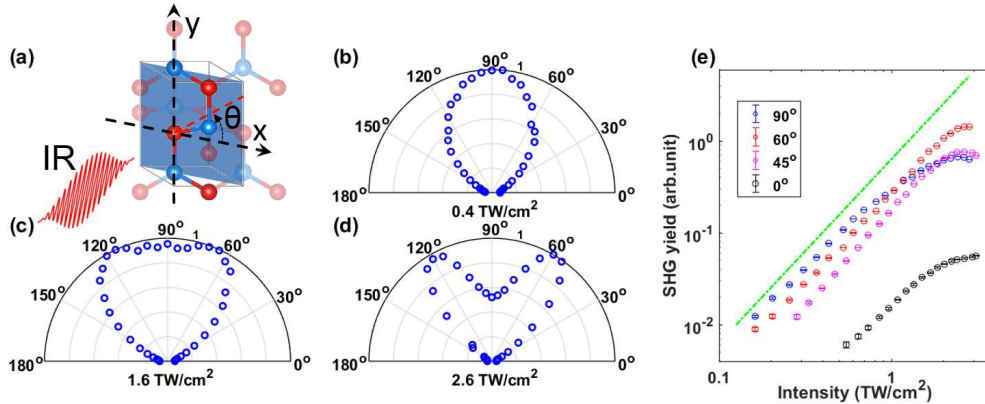


FIG. 1. (a) The schematic diagram of our experiments. (b)-(d) Orientation dependence of the SHG under the laser intensities (b) 0.4 TW/cm^2 , (c) 1.6 TW/cm^2 , and (d) 2.6 TW/cm^2 . The laser wavelength is 2300 nm . The results are normalized to one. (e) Laser intensity dependence of SHG yield at different orientations. The dashed lines mark the scaling of I^2

is lower than 0.6 TW/cm^2 , the SHG yield obeys the scaling law of I^2 and the structures of the orientation-dependent SHG are near unchanged. However, the scalings show obvious deviations from I^2 with increasing the laser intensity. Strikingly, the deviation occurs at 0.8 TW/cm^2 for 90° and at higher intensities (1.4 TW/cm^2 and 1.9 TW/cm^2) for 45° and 60° , which leads to the fat “8” and butterfly structure in Fig. 1(c) and 1(d).

To get a deeper insight, we further observe the different polarization components of the SHG. The first row in Fig. 2 shows the orientation dependence of y-component, and the second row shows the results of x-component. We have confirmed that the SHG along the propagation direction (i.e., z-direction) is negligible (see Sec. II in the supplementary information). As shown in Figs. 2(a)-2(c), the y-component shows an “8” structure, and the structure is almost unchanged with increasing the laser intensity. The scalings of the y-component at four typical orientations are also shown in Fig. 2(d). One can see that the scalings are nearly I^2 below 0.8 TW/cm^2 , and then become saturated. In contrast, the x-component behaves totally differently as shown in Figs. 2(e)-2(h). Firstly, the orientation dependence of the x-component shows a butterfly structure, and the location of the peaks changes from 45° (135°) to about 60° (120°) with increasing the laser intensity. Secondly, the scalings are approximate I^2 below 0.6 TW/cm^2 and then show up an exponential growth with increasing the laser intensity until the saturation at around 2 TW/cm^2 . Moreover, the

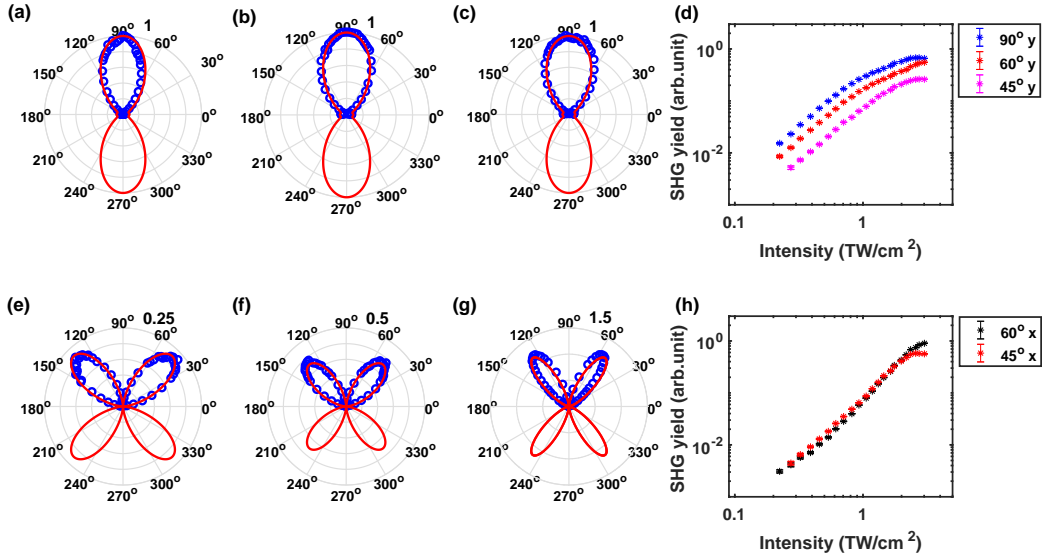


FIG. 2. The y-component SHG under the laser intensities (a) 0.4 TW/cm^2 , (b) 1.6 TW/cm^2 , and (c) 2.6 TW/cm^2 . (d) Laser intensity dependence of y-component SHG yield at different orientations. The x-component SHG under the laser intensities (e) 0.4 TW/cm^2 , (f) 1.6 TW/cm^2 , and (g) 2.6 TW/cm^2 . (h) Laser intensity dependence of x-component SHG yield at different orientations. The laser wavelength is 2300 nm .

x-component gradually dominates over the y-component above 2 TW/cm^2 . These results indicate that the change of the orientation distribution of SHG in Fig. 1 mainly results from the x-component SHG, which is obviously dependent on the laser intensity. To the best of our knowledge, these phenomena have never been reported in previous experiments, and the normal nonlinear optics theory does not predict such intensity-dependent modifications of SHG.

The above results in Figs. 1 and 2 indicate the breakdown of the normal nonlinear optics theory with increasing the laser intensity. To give an intuitive picture underlying the experimental observation, we consider the nonlinear polarization with the bond-charge model (BCM) [4]. According to the BCM, the susceptibility of a whole system can be predicted by summing the responses of various bonds present in the material. For the ZnO crystal used in our experiment, there are 4 equivalent Zn-O bonds in a unit cell on the laser polarization plane (x-y plane, see Fig. 3(a)). The outer electrons are mostly localized within the bonds that confine the atoms to their lattice sites. The driving electric field induces the

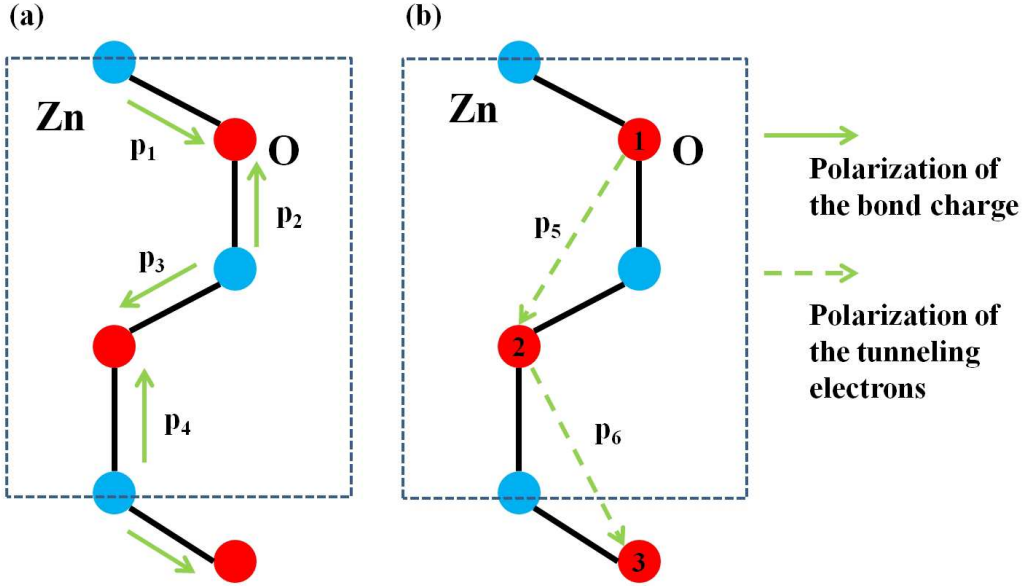


FIG. 3. The sketch of the nonlinear polarization in ZnO. We show the crystal structure of ZnO in the x-y plane, and the dotted box marks a unit cell. (a) The solid arrows (\mathbf{p}_1 , \mathbf{p}_2 , \mathbf{p}_3 , and \mathbf{p}_4) mark the second-order nonlinear polarization contributed by the inherent Zn-O bonds. (b) The dashed arrows (\mathbf{p}_5 and \mathbf{p}_6) mark the second-order nonlinear polarization contributed by the tunneling electrons.

nonlinear dipole along with the Zn-O bonds and the second-order nonlinear polarizations are denoted as \mathbf{p}_m , $m = 1, 2, 3, 4$. In this case, the hyperpolarizabilities of these four bonds are equal and the amplitudes are set to β^0 . By summing the responses of all four bonds and taking account of the orientation of each bond, one can obtain the second-order nonlinear polarization $\mathbf{P}^0 = \sum_{m=1}^4 \mathbf{p}_m = \chi^{(2)} \mathbf{E} \mathbf{E}$ and the second-order susceptibility $\chi^{(2)}$ is (see Sec. IV in the supplementary information)

$$\begin{bmatrix} P_x \\ P_y \end{bmatrix} = \chi^{(2)} \mathbf{E} \mathbf{E} = \beta^0 \begin{bmatrix} 0 & 0 & -0.5590 \\ -0.5590 & 1.9410 & 0 \end{bmatrix} \begin{bmatrix} E_x E_x \\ E_y E_y \\ 2E_x E_y \end{bmatrix} \quad (1)$$

Here we only show the elements in the laser polarization plane, because the SHG along the propagation direction is negligible.

In the strong laser field, the electrons within nearby bonds can be coupled by quantum tunneling. For ZnO, the upmost valence electrons are primarily from the 2p orbital of

oxygen atoms. Therefore, the tunneling is mainly contributed by the valence electrons near oxygens. We consider that the tunneling between the nearest oxygens is dominant, because the barriers between the next-neighbor oxygens are wider, and have a much smaller tunneling probability. There are mainly two kinds of tunneling events in one unit cell of ZnO. The first one is the tunneling between oxygen 1 and oxygen 2 (refer to O1, O2), e.g., electron near the O1 tunnels to O2, and a hole is left near O1. This effect can induce an additional polarization to the normal Zn-O bonds. The second tunneling occurs between O2 and O3. Note that tunneling is a nonperturbative effect, we call it NPBM and denote the nonlinear polarization induced by tunneling electrons to \mathbf{p}_5 and \mathbf{p}_6 (see Fig. 3(b)). The tunneling depends sensitively on the driving laser, and therefore, their hyperpolarizabilities are laser-dependent too, which are denoted as $\beta_5(E_0, \theta)$ and $\beta_6(E_0, \theta)$. Finally, one can write the second-order nonlinear polarization by using the susceptibilities, $\mathbf{P}' = \mathbf{p}_5 + \mathbf{p}_6 = \chi^{(2)}\mathbf{E}\mathbf{E}$, that is (see Sec. V in the supplementary information),

$$\begin{bmatrix} P'_x \\ P'_y \end{bmatrix} = \chi'^{(2)}\mathbf{E}\mathbf{E} = \begin{bmatrix} 0.4061\beta^- & 0.7694\beta^- & -0.5590\beta^+ \\ 0 & 0 & 0 \end{bmatrix} \begin{bmatrix} E_x E_x \\ E_y E_y \\ 2E_x E_y \end{bmatrix} \quad (2)$$

where $\beta^- = \beta_6(E_0, \theta) - \beta_5(E_0, \theta)$, and $\beta^+ = \beta_6(E_0, \theta) + \beta_5(E_0, \theta)$. Note that, due to the tunneling effect, the depletion of the bond charge of normal Zn-O bond will decrease the hyperpolarizability β^0 with increasing laser intensity. We denote the population of tunneling electron is ρ_e . Then the total second-order nonlinear polarization is $\mathbf{P} = (1 - \rho_e)\mathbf{P}^0 + \rho_e\mathbf{P}'$. We can define a GSOS for the second-order nonlinear polarization in the strong fields,

$$\eta_{ijk}^{(2)}(\beta^0, \beta^+, \beta^-) = (1 - \rho_e)\chi_{ijk}^{(2)}(\beta^0) + \rho_e\chi'_{ijk}{}^{(2)}(\beta^+, \beta^-) \quad (3)$$

Before explaining the experiment, we briefly summarize the property of the proposed GSOS. First, when the laser field is weak, ρ_e and the tunneling induced polarization can be neglected, and the hyperpolarizability β^0 is a laser-independent constant, which goes back to the normal second-order susceptibility. With increasing the laser intensity, the first term decreases, but the second term has a similarly exponential growth with the tunneling probability (see Sec. V in the supplementary information) and becomes dominant gradually. More importantly, the tunneling induced polarization leads to new nonvanishing elements compared with the normal SOS, which will remarkably influence the anisotropy of SHG.

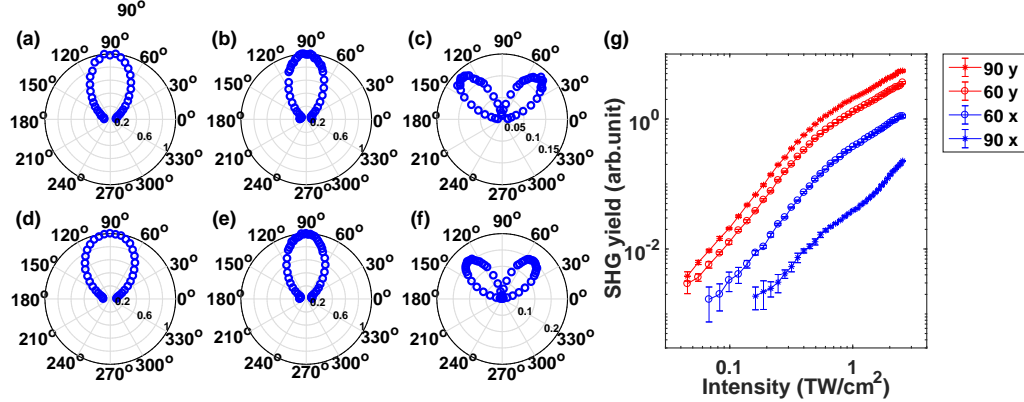


FIG. 4. Anisotropic second harmonic generation with 800-nm lasers. The total (first column), y-component (second column), and x-component (third column) SHG under laser intensity (a)-(c) 0.1 TW/cm² and (d)-(f) 1.6 TW/cm². (g) Laser intensity dependence of x-component and y-component SHG yield at different orientations.

Next, we discuss the role of tunneling induced polarization on different components of SHG. According to Eqs. (1) and (2), one can see that the y-component SHG is only contributed by the inherent term $\chi^{(2)}(\beta^0)$. As shown in Figs. 2(a)-2(d), the orientation dependencies of the y-component SHG are nearly unchanged with increasing the laser intensity, and the scalings also follow similar trends. These phenomena are in good accordance with the results from GSOS (red lines), and the hyperpolarizability β^0 can be obtained by fitting the experimental results. On the other hand, the x-component SHG can be contributed by both the inherent term $\chi^{(2)}(\beta^0)$ and the tunneling induced term $\chi'^{(2)}(\beta^+, \beta^-)$. For $\chi^{(2)}(\beta^0)$, according to Eq. (1), only the term $\chi_{xxy}^{(2)}$ contributes to the x-component SHG, and its structure is determined by $|2E_x E_y|^2$, which has a butterfly shape with peaks at 45°, 135°, etc. Different from that, the contribution from the tunneling induced term $\chi'^{(2)}(\beta^+, \beta^-)$ depends on the laser parameters.

Following the above discussions, we explain how to understand the experimental observations by using the GSOS. According to Eqs. (1), (2) and (3), we can rewrite the GSOS as

$$\eta^{(2)} = k_0 \begin{bmatrix} 0 & 0 & -0.5590 \\ -0.5590 & 1.9410 & 0 \end{bmatrix} + \begin{bmatrix} 0.4061k^- & 0.7694k^- & -0.5590k^+ \\ 0 & 0 & 0 \end{bmatrix} \quad (4)$$

where $k_0 = (1 - \rho_e)\beta^0$, and $k^\pm = \rho_e\beta^\pm$. For simplicity, we normalize the maximum of the y-component SHG to 1. As discussed above, the y-component SHG is only contributed by

$\chi^{(2)}(\beta^0)$. By fitting the normalized y-component SHG, a normalization parameter $k_0 = 0.515$ can be obtained. Then, we only need two unknown parameters k and σ to describe the tunneling induced terms $\chi'^{(2)}(\beta^+, \beta^-)$. In details, the tunneling probability can be modeled by $k^\pm = \rho_e \beta^\pm = k \left[\frac{\alpha_5}{\max(\alpha_5)} \pm \frac{\alpha_6}{\max(\alpha_6)} \right]$, where $\alpha_{5,6} = e^{\sigma(E_0) |\cos(\theta - \theta_{5,6})|^2}$. The parameter k describes the weight, and the parameter $\frac{\alpha_{5,6}}{\max(\alpha_{5,6})}$ determines the orientation dependence. By fitting with the experimental result of x-component SHG (Fig. 2(e)-(g)), one can obtain the optimal fitting parameters $k = 0.17, 0.30, 0.78$, and $\sigma = 0.20, 1.08, 5.06$, for different laser intensities 0.4, 1.6, and 2.6 TW/cm², respectively. In our fitting scheme, the birefringent effect in the crystal ZnO has been involved by introducing a phase different $\Delta\varphi = 0.83$ between the x- and y-component of the fundamental electric field (see Sec. III in the supplemental information). The results from our model are plotted by red lines in Figs. 2(e)-2(g), which agree well with the experimental results.

The contribution of the laser-induced term is proportional to the population of the tunneling electrons. Its contribution will be decreased if using a shorter wavelength laser because the electron can not obtain high enough energy to tunnel through the potential barrier. To demonstrate this idea, we repeat the experiments using the 800-nm laser pulse. As shown in Fig. 4, with decreasing the wavelength, the changes of the orientation dependencies of SHG become less remarkable. Although the relative strength of the x-component SHG is increased with increasing the laser intensity, it is still much weaker than that of y-component SHG (see Figs. 4(c), 4(f) and 4(g)). Therefore, the orientation dependencies of total SHG only show imperceptible changes and always show the "8" structure until the damage intensity (see Figs. 4(a) and 4(d)). This result supports our model again and also explains why the phenomena in our experiments were not observed in previous works with a routinely used Ti:Sapphire laser.

In conclusion, we demonstrate the so far overlooked polarization induced by strong-field tunneling as a new source of nonlinear polarization. It can be explained by the NPBCM and GSOS by taking account of the tunneling between the neighboring bonds. Our work covers the edge between normal and strong field nonlinear optics. Different from the normal second-order susceptibility, the GSOS involves a laser dependent term that can be modified by changing the laser intensities and wavelengths. We can envisage achieving the nonlinear optics control in the attosecond time scale by using a few-cycle pulse [11, 16] or two-color pulse [24, 25]. It suggests an all-optical approach to control the nonlinear responses with

high switching rate and paves the ways for achieving the ultrafast optical switching.

This paper was supported by the National Key R&D program (2017YFE0116600) and National Natural Science Foundation of China (NSFC) (No. 91950202, 12021004, 11934006, 11627809, 11874165). Numerical simulations presented in this paper were carried out using the High Performance Computing experimental testbed in SCTS/CGCL.

-
- [1] P. A. Franken, A. E. Hill, C. W. Peters, and G. Weinreich, *Phys. Rev. Lett.* **7**, 118 (1961).
 - [2] N. Bloembergen, and P. S. Fershan, *Phys. Rev.* **128**, 606 (1962).
 - [3] J. A. Armstrong, N. Bloembergen, J. Ducuing, and P. S. Pershan, *Phys. Rev.* **127**, 1918-1939 (1962).
 - [4] R. W. Boyd, *Nonlinear optics*, (Academic Press, Boston, MA) 2008
 - [5] Y. R. Shen, *The principles of nonlinear optics* (Wiley, New York) 1984.
 - [6] A. McPherson, G. Gibson, H. Jara, U. Johann, T. S. Luk, I. A. McIntyre, K. Boyer, and C. K. Rhodes, *J. Opt. Soc. Am. B* **4** 595(1987)
 - [7] M. Ferray, A. L. Huillier, X. F. Li, L. A. Lompre, G. Mainfray, and C. Manus, *J. Phys. B* **21** L31 (1988)
 - [8] S. Ghimire, A. D. DiChiara, E. Sistrunk, P. Agostini, L. F. DiMauro, and D. A. Reis, *Nat. Phys.* **7**, 138-141 (2011).
 - [9] P. Jürgens, et al., *Nat. Phys.* **16** 1035-1039 (2020).
 - [10] T. T. Luu, M. Garg, S. Yu. Kruchinin, A. Moulet, M. Th. Hassan, and E. Goulielmakis, *Nature* **521**, 498-502 (2015).
 - [11] O. Schubert, et al., *Nat. Photon.* **8**, 119-123 (2014).
 - [12] G. Ndabashimiye, S. Ghimire, M. Wu, D. A. Browne, K. J. Schafer, M. B. Gaarde, and D. A. Reis, *Nature* **534**, 520-523 (2016).
 - [13] Y. S. You, D. A. Reis, and S. Ghimire, *Nat. Phys.* **13**, 345 (2016).
 - [14] T.T. Luu, Z. Yin, A. Jain, T. Gaumnitz, Y. Pertot, J. Ma, and H. J. Wörner, *Nat. Commun.* **9**, 3723 (2018).
 - [15] <https://www.nature.com/milestones/milephotons/timeline.html>
 - [16] M. Schultze, et al., *Nature* **493**, 75 (2013).
 - [17] M. Lenzner, J. Krüger, S. Sartania, Z. Cheng, Ch. Spielmann, G. Mourou, W. Kautek, and

- F. Krausz, Phys. Rev. Lett. **80**, 4076-4079 (1998).
- [18] S. Ghimire, A. D. DiChiara, E. Sistrunk, U. B. Szafruga, P. Agostini, L. F. DiMauro, and D. A. Reis, Phys. Rev. Lett. **107**, 167407 (2011).
- [19] M. Durach, A. Rusina, M. F. Kling, and M. I. Stockman, Phys. Rev. Lett. **107**, 086602 (2011)
- [20] M. Th. Hassan, et al., Nature **530**, 66-70 (2016).
- [21] G. Vampa, et al., Nat. Photon. **12**, 465-468 (2018).
- [22] A. Schiffrin, et al., Nature **493**, 70-74 (2013).
- [23] T. Higuchi, C. Heide, K. Ullmann, H. B. Weber, and P. Hommelhoff, Nature **550**, 224-228 (2017).
- [24] P. Lan, P. Lu, W. Cao, Y. Li, and X. Wang, Phys. Rev. A **76**, 051801(R) (2007).
- [25] K. J. Betsch, D. W. Pinkham, R. R. Jones, Phys. Rev. Lett. **105**, 223002 (2010).